Performance analysis of precoded layered ACO-OFDM for visible light communication systems

Ali Waqar Azim, Yannis Le Guennec, Ghislaine Maury

Version of Record: https://www.sciencedirect.com/science/article/pii/S0030401819301002
Manuscript_90ca41cc66a6a7d9a1e567e421bb514c

Performance Analysis of Precoded Layered ACO-OFDM for Visible Light Communication Systems

Ali W. Azim[a,*], Yannis Le Guennec[a], Ghislaine Maury[b]

[a] *Université Grenoble Alpes, CNRS, Institute of Engineering, Grenoble INP, GIPSA-LAB, 38000 Grenoble, France*
[b] *Université Grenoble Alpes, CNRS, Institute of Engineering, Grenoble INP, IMEP-LAHC, 38000 Grenoble, France*

Abstract

Optical-orthogonal frequency division multiplexing (O-OFDM) is regarded as an effective scheme for intensity modulation and direct detection (IM-DD) based visible light communication (VLC) systems. State-of-the-art O-OFDM approaches complying with IM-DD constraints are; direct-current (DC) biased O-OFDM (DCO-OFDM) and asymmetrically clipped (AC)O-OFDM. ACO-OFDM has half the spectral efficiency (SE) of DCO-OFDM, howbeit, its SE can be augmented towards that of DCO-OFDM using layered ACO-OFDM (LACO-OFDM). Nevertheless, LACO-OFDM suffers from a high peak-to-average power ratio (PAPR). Forthright extension of PAPR reduction techniques devised for ACO-OFDM to LACO-OFDM can be unwieldy and complex. Hence, precoding can be an alternative to counterbalance the high PAPR without a considerable increase in complexity. As our contribution, we comprehensively investigate the performances of Fourier transform (FT) and Hartley transform (HT) precoding on LACO-OFDM. The bit error rate (BER) is analyzed in additive white Gaussian noise (AWGN) and time dispersive channels. Furthermore, the impact of superimposition of layers, PAPR, electrical-to-optical power conversion efficiency and system complexities are also investigated.

Keywords: Intensity modulation-direct detection, optical-orthogonal frequency division multiplexing, peak-to-average power ratio, asymmetrically-clipped optical-orthogonal frequency division multiplexing.

1. Introduction

Over the preceding couple of decades, there has been an exponential expansion in deployment of radio frequency (RF) wireless systems. Owing to an inflated demand for data hungry wireless applications, considerable amount of RF spectrum is being used. Moreover, it is subjected to an excessive spatial re-use, which has elevated co-channel interferences and have led to serious quality-of-service concerns. On the other hand, the wireless network traffic is growing, henceforth, there is

*Corresponding author. Tel./fax: +33-660-380-994
Email addresses: aliwaqar.azim@grenoble-inp.fr (Ali W. Azim), yannis.le-guennec@grenoble-inp.fr (Yannis Le Guennec), ghislaine.maury@grenoble-inp.fr (Ghislaine Maury)

a substantiated need to unburden the dwindling RF spectrum. Visible light communication (VLC) is perceived as a possible complementary technology to the impending RF spectral crisis. With some compelling advantages, such as, license free virtually unlimited bandwidth, high-security, no electromagnetic interference/pollution, energy efficient green communication with low carbon dioxide (CO_2) footprint, VLC is alluring as it offers both lighting and communication simultaneously [1].

Optical-orthogonal frequency division multiplexing (O-OFDM) is regarded as an effective technique for VLC; as it can attain high data-rate by exploiting multiple orthogonal subcarriers to transmit parallel data streams; eliminates the demand for complex equalizers; and embodies an inherent resilience to combat inter-symbol-interference [2–5]. O-OFDM in VLC can be implemented using simple, low-cost intensity modulation and direct detection (IM-DD), wherein, the intensity waveform is modulated onto the brightness of the light-emitting diode (LED) and these variations in light intensity are photo-detected at the receiver using direct-detection. For IM-DD implementation, the time-domain (TD) signal is constrained to be real-valued and non-negative. To achieve a real-valued signal, Hermitian symmetry (HS) is generally administered in the frequency-domain (FD), the resulting TD signal is real-valued but bipolar. Numerous strategies exist to obtain a non-negative signal. A forthright approach is to incorporate a bias to exclude the negative excursions, nevertheless, the addition of bias translates to an energy inefficacy. The approach of adding a bias to a bipolar TD O-OFDM signal is referred to as direct-current (DC) biased O-OFDM (DCO-OFDM) [2]. Other approaches capitalize on the frame structure of O-OFDM (either in TD or FD) to realize a non-negative TD. These approaches include asymmetrically clipped (AC)O-OFDM [3], pulse-amplitude-modulation-discrete multi-tone (PAM-DMT), Flip-OFDM [6] and unipolar (U)-OFDM [7], etc. In ACO-OFDM and PAM-DMT, an anti-symmetric TD signal is generated by taking advantage of on a unique frame structure in FD, for which, the negative amplitude excursions are clipped to zero without loss of information. In Flip-OFDM and U-OFDM, the positive and the reversed-negative samples of the bipolar signals are successively transmitted. These approaches (which do not use bias) are power efficient compared to DCO-OFDM only for lower spectral efficiencies, but surrender their power advantage for higher spectral efficiencies.

The non-negative signal generation process for ACO-OFDM, PAM-DMT, Flip-OFDM, and U-OFDM halves the spectral efficiency (SE) compared to DCO-OFDM. This SE reduction is either due to the halving of the modulated subcarriers or doubling the transmit time of a symbol. To augment the SE of these approaches towards that of DCO-OFDM and to retain their power advantage over DCO-OFDM for higher spectral efficiencies, the so-called *hybrid* approaches have been proposed. The hybrid counterpart of ACO-OFDM is the layered ACO-OFDM (LACO-OFDM) [8, 9], which stacks layers of ACO-OFDM; with each succeeding layer modulating the empty subcarriers left by the preceding layers. Augmented SE-DMT (ASE-DMT) [10] and enhanced U-OFDM (eU-OFM) [11] are hybrid counterparts of PAM-DMT and U-OFDM/Flip-OFDM, respectively. Regardless, some of the hybrid approaches might face some pragmatic limitations, e.g., Lowery [12] identified that eU-OFDM might need complex TD equalization process along with additional cyclic prefixes between the positive and the negated-negative frames to avoid the interference between the positive

and negative components. Nonetheless, according to [9], among these hybrid techniques, LACO-OFDM brings greater flexibility in design, since, the number of layers, modulation cardinality and power allocation to each layer can be regulated as needed [9]. Henceforth, in the sequel, we shall only consider LACO-OFDM and its precoded variants.

Despite of advantages, LACO-OFDM experiences high peak-to-average-power ratio (PAPR); which may exacerbate the non-linear distortions from the LED [13, 14]. Limited resolution digital-to-analog converter (DAC) can further delineate the performance [13]. Albeit, many methods exist to alleviate the high PAPR of O-OFDM (e.g., [13, 15, 16]), but, their candid implementation to hybrid techniques is unwieldy. Recently, Zhang *et al.* [9] introduced a tone injection based PAPR reduction approach for LACO-OFDM, however, it is accompanied with a considerable complexity overhead. An alternative to scale down the high PAPR is to use precoding; because it proceeds in a quasi single-carrier like behavior resulting in a lower PAPR and does not inflict significant complexity overhead. In the literature, Fourier transform (FT)-precoded ACO-OFDM (FTP-ACO-OFDM) [17–19] and Hartley transform (HT)-precoded ACO-OFDM (HTP-ACO-OFDM) [20] are investigated; which manifest lower PAPR compared to non-precoded counterpart. It may be noticed that, FTP-ACO-OFDM is identical to ACO-OFDM with a sole exception that the modulation alphabets are FT precoded before being mapped onto the subcarriers. In HTP-ACO-OFDM, HS is precluded because of real-valued HT and the use of PAM alphabets. Ranjha *et al.* analyzed the performance of precoding on ACO-OFDM and PAM-DMT [19]. However, the layered formation culminates in different performances for precoded and non-precoded approaches, thus, the conclusions rendered in [19] cannot be drawn-out for the layered counterparts.

In the literature, two distinctive techniques with FT precoding for LACO-OFDM have been proposed in [21]. Among them, one adheres to the HS constraint, i.e., FTP-LACO-OFDM, while, the other averts it; which is referred to as real-imaginary (RI)-interleaved DFT-spread (IDFTS). In terms of performance, only the PAPR manifested by FTP-LACO-OFDM and RI-IDFTS is different, with RI-IFTS exhibiting significantly lesser PAPR compared to FTP-LACO-OFDM. Nonetheless, RI-IDFTS might face some significant limitations in practical scenarios. For example, it employs real and imaginary separation (RIS) at the transmitter to attain a real-valued non-negative signal for transmission. However, it is necessaet that the real and the imaginary components must not interfere with one another in a bandwidth-limited channel after RIS, otherwise, a significantly complex equalization process might be required. On the other hand, FTP-LACO-OFDM does not face this issue because RIS is not required. Moreover, for RI-IDFTS at the receiver to perform inverse RIS, strict synchronization for the received samples is necessary; which might considerably increase the cost of the system. Another vital demerit is significant complexity overhead for both FTP-LACO-OFDM and RI-IDFTS. In this context, Khalighi *et al.* [14] have highlighted the same issue [1]. In the article, we shall demonstrate that FTP-LACO-OFDM and RI-IDFTS are compu-

[1]In [14], the authors discuss about eU-OFDM. Nonetheless, the computational complexity of eU-OFDM and LACO-OFDM is the same, hence, the conclusions regarding computational complexity of eU-OFDM can be generalized for LACO-OFDM.

tationally more complex than conventional LACO-OFDM. However, for the sake of comparison, we shall primarily employ FTP-LACO-OFDM; which is the layered variant of FTP-ACO-OFDM presented in [17–19] . HTP variants of LACO-OFDM have been studied in [22] and [23]; which have also shown to manifest lower PAPR than LACO-OFDM. Howbeit, these investigations have a few shortcomings, e.g., in [21], the authors have not presented the bit error rate (BER) performance considering a time dispersive channel; which consists of a multipath VLC scattering and bandwidth limitation of LED/LED driver combo. Additionally, the optical power penalty with respect to on-off keying (OOK), the complexity of the FTP layered approaches, electrical-to-optical power conversion efficiency, and the attenuation anticipated due to the layered structure, i.e., layering attenuation have been disregarded. Moreover, in [22] and [23], the BER performance considering optical signal-to-noise ratio (SNR), electrical-to-optical power conversion efficiency and layering attenuation have not been analyzed. Moreover, in [22], the study of the optical power penalty in a time dispersive channel is not provided, and [23] does not appraise the impact of the number of layers on PAPR and the impact of non-linear distortions on BER.

Hereby, in this article, we have sought to fill in the gaps in performance analysis of precoded and non-precoded LACO-OFDM approaches. For this purpose, we shall consider LACO-OFDM, FTP-LACO-OFDM and HTP-LACO-OFDM. We shall also use RI-IDFTS to illustrate the PAPR performance with respect to different alphabet cardinalities. To the best of our knowledge, an exhaustive performance analysis is not available in the literature. The performance criteria recognized are: the layering attenuation, electrical-to-optical power conversion efficiency, the SE, the BER performance in additive white Gaussian noise (AWGN) and time dispersive channels considering both electrical and optical SNRs, the affect of number of layers on PAPR, the impact of non-linear distortions on BER, the optical power penalty with respect to OOK and computational complexity.

The rest of the article is organized as follows. In section 2, we present the fundamentals of discrete FT (DFT), inverse DFT (IDFT), discrete HT (DHT), inverse DHT (IDHT) and the system model. In section 3, we present LACO-OFDM, FTP-LACO-OFDM and HTP-LACO-OFDM approaches. Section 4 analyzes the performance of aforementioned schemes for different performance parameters. Section 5 compares the performances of LACO-OFDM and its precoded variants. Conclusions are rendered in section 6.

1.1. Notation

We use *uppercase* letters with index k and *lowercase* letters with index n to represent kth and nth sample of N-length FD and TD signals, respectively, e.g., $S(k)$ and $s(n)$. For lth layer FD and TD signals (which are not N-length), we adopt indices $k^{(l)}$ and $n^{(l)}$. *Boldface uppercase calligraphic* letters, $\boldsymbol{\mathcal{Q}}$ and $\boldsymbol{\mathcal{P}}$ represent quadrature-amplitude modulation (QAM) and PAM constellation sets. $\mathbb{C}$ and $\mathbb{R}$ describe the complex-valued and the real-valued signals, respectively. We use $E(\cdot)$, $(\cdot)^*$, $\lfloor\cdot\rfloor$ and $\otimes$ to indicate the ensemble average, complex conjugate, zero level clipping and convolution operators, respectively. LACO, FTP and HTP in the subscript of a parameter, e.g., $(\cdot)_{\text{LACO}}$, $(\cdot)_{\text{FTP}}$

and $(\cdot)_{\text{HTP}}$ are employed to identify between LACO-OFDM, FTP-LACO-OFDM and HTP-LACO-OFDM. Alternatively, for brevity, we use $(\cdot)$ in the subscript of a parameter to indicate all the techniques, e.g., $\alpha_{(\cdot)}$ means α_{LACO}, α_{FTP} and α_{HTP}.

2. Preliminaries

To facilitate the notation in the sequel, we present DFT/IDFT, DHT and IDHT. Afterward, we shall present the system model.

2.1. Transforms

N-order DFT for an arbitrary TD signal, $r(n) \in \mathbb{C}$ is given as:

$$R(k) = \text{DFT}\left[r(n)\right] = \frac{1}{\sqrt{N}} \sum_{n=0}^{N-1} r(n) \exp\left(\frac{-j2\pi nk}{N}\right), \tag{1}$$

where $k = 0, 1, \cdots, N-1$ and $j = \sqrt{-1}$. Whereas, N-order IDFT for an arbitrary FD signal $R(k) \in \mathbb{C}$ reads:

$$r(n) = \text{IDFT}\left[R(k)\right] = \frac{1}{\sqrt{N}} \sum_{k=0}^{N-1} R(k) \exp\left(\frac{j2\pi nk}{N}\right), \tag{2}$$

for $n = 0, 1, \cdots, N-1$. Traditionally, O-OFDM approaches use IDFT/DFT for multiplexing/demultiplexing of the subcarriers. An alternative is to adopt IDHT/DHT (as in HTP-ACO-OFDM) if the input alphabets are drawn from real-valued constellations, e.g., PAM. N-order DHT for an arbitrary real-valued TD signal, $r(n) \in \mathbb{R}$, is

$$R(k) = \text{DHT}\left[r(n)\right] = \frac{1}{\sqrt{N}} \sum_{n=0}^{N-1} r(n)\text{cas}\left(\frac{2\pi kn}{N}\right), \tag{3}$$

where $k = 0, 1, \cdots, N-1$ and $\text{cas}(\cdot) = \cos(\cdot) + \sin(\cdot)$. N-order IDHT for an arbitrary FD signal, $R(k) \in \mathbb{R}$ is given as:

$$r(n) = \text{IDHT}\left[R(k)\right] = \frac{1}{\sqrt{N}} \sum_{k=0}^{N-1} R(k)\text{cas}\left(\frac{2\pi kn}{N}\right), \tag{4}$$

where $n = 0, 1, \cdots, N-1$. The kernel for both DHT and IDHT is interchangeable, hence, same algorithm can drive both processes [20]. Besides, real-valued input to DHT/IDHT result in a real-valued output; this could be advantageous because a real-valued TD signal would be attained without involving HS. On the other hand, HS is required in the FD to realize a real-valued TD signal if DFT/IDFT are used; which may involve substantial computational resources [24].

2.2. System Model

Let $x(t)$ be the data-carrying intensity waveform which modulates the brightness of the LED; and is obtained after digital to analog conversion of $x(n)$[2]. $x(t)$ is transformed to an optical intensity signal, $u(t) = \varepsilon x(t)$, where ε (Watt/Ampere) is the electrical-to-optical conversion factor. For simplicity, we consider ideal synchronization [13, 25]. The LED non-linearity can be lessened using digital pre-distortion [26], henceforth, a linear response for the LED is adopted between turn-on current and saturation current. The photo-detected signal is $g(t) = \kappa u(t)$, where κ (Ampere/Watt) is the responsitivity of the photo-diode (PD). Without loss of generality, we consider $\varepsilon = 1$ (Watt/Ampere) and $\kappa = 1$ (Ampere/Watt), hence, $g(t) = u(t) = x(t)$. The channel realizations are $h(t)$. The received signal is contaminated by the ambient noise, $w(t)$, thus, we have

$$y(t) = h(t) \otimes x(t) + w(t), \tag{5}$$

where $w(t)$ is modeled as AWGN with mono-lateral power spectral density (PSD) of N_0.

After impinging $y(t)$ on an analog-to-digital converter (ADC), the sampled version, $y(n)$ for $n = 0, 1, \cdots, N-1$ is obtained. By feeding $y(n)$ to N-order DFT, the FD counterparts of $y(n)$ for LACO-OFDM and FTP-LACO-OFDM are obtained as [17–19]:

$$Y(k) = H(k)X(k) + W(k), \tag{6}$$

for $k = 0, 1, \cdots, N-1$. For HTP-LACO-OFDM, $y(n)$ is transformed into FD via N-order DHT as [22, 23]:

$$Y(k) = H^{\mathrm{e}}(k)X(k) + H^{\mathrm{o}}(k)X(N-k) + W(k), \tag{7}$$

for $k = 0, 1, \cdots, N-1$. For LACO-OFDM and FTP-LACO-OFDM, $H(k) = \mathrm{DFT}[h(n)]$, whereas, for HTP-LACO-OFDM, $H(k) = \mathrm{DHT}[h(n)] = H^{\mathrm{e}}(k) + H^{\mathrm{o}}(k)$, with $H^{\mathrm{e}}(k) = N^{-1/2} \sum_{n=0}^{N-1} h(n) \cos(2\pi kn/N)$ and $H^{\mathrm{o}}(k) = N^{-1/2} \sum_{n=0}^{N-1} h(n) \sin(2\pi kn/N)$ for $\{k, n\} = 0, 1, \cdots, N-1$. $Y(k)$, $X(k)$ and $W(k)$ are the FD counterparts of $x(n)$, $y(n)$ and $w(n)$, respectively. (6) differs for (7) because unlike DFT property, the convolution in TD is not multiplication in Hartley domain. Thence, the equalization process for HTP-LACO-OFDM differs from that of LACO-OFDM and FTP-LACO-OFDM; and can be implemented as reported in [22, 27]. On the other hand, zero-forcing (ZF) and minimum mean-square error (MMSE) equalization can be implemented for LACO-OFDM and FTP-LACO-OFDM. The equalization complexity for HTP-LACO-OFDM is the same as that ZF equalization for LACO-OFDM [22]. After equalization on $Y(k)$, the following FD signal is realized:

$$\hat{Y}(k) = \hat{X}(k) + Z(k), \tag{8}$$

where $Z(k) = W(k)/H(k)$ is the noise colored by the frequency response of the channel.

[2]For brevity, we consider that $x(n)$ also incorporates cyclic prefix (CP) of length N_{CP}.

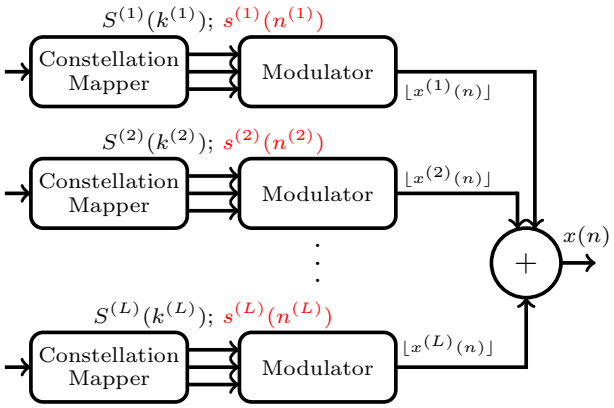

Figure 1: Transmitter configuration for the layered approaches. The input to the modulator is expressed in black and red, respectively for LACO-OFDM and procoded LACO-OFDM (FTP-LACO-OFDM and HTP-LACO-OFDM).

3. Layered ACO-OFDM and Precoding

We shall now present LACO-OFDM, FTP-LACO-OFDM and HTP-LACO-OFDM considering N subcarriers (which is typically a power of 2, i.e., 2^i, where i is an integer), and L layers. Generalized transmitter and receiver configurations for precoded and non-precoded LACO-OFDM methods are presented in Fig. 1 and Fig. 2, respectively. The block diagram of modulators for ACO-OFDM, FTP-ACO-OFDM and HTP-ACO-OFDM are depicted in Fig. 3.

3.1. LACO-OFDM

3.1.1. Transmitter

For the lth layer, the incoming bit stream is mapped onto M-ary QAM FD symbols, $S^{(l)}\left(k^{(l)}\right), k^{(l)} = 0, 1, \cdots, N/2^{l+1} - 1$, chosen from constellation set $\boldsymbol{\mathcal{Q}} = \{\mathcal{Q}_0, \mathcal{Q}_1, \cdots, \mathcal{Q}_{M-1}\}$. $S^{(l)}\left(k^{(l)}\right)$ are then allocated to N-length signal, $X^{(l)}(k), k = 0, 1, \cdots, N-1$ by complying to HS as:

$$X^{(l)}(k) = \begin{cases} S^{(l)}(k^{(l)}), & k = 2^{l-1}(2k^{(l)} + 1) \\ S^{*(l)}(k^{(l)}), & k = N - 2^{l-1}(2k^{(l)} + 1) \\ 0, & \text{elsewhere} \end{cases} . \tag{9}$$

A TD signal is obtained via N-order IDFT as:

$$x^{(l)}(n) = \text{IDFT}\left[X^{(l)}(k)\right], \tag{10}$$

for $n = 0, 1, \cdots, N-1$. For all the layers, the signal, $x^{(l)}(n)$ is anti-symmetric, i.e.,

$$x^{(l)}(\tilde{n}^{(l)}) = -x^{(l)}\left(\tilde{n}^{(l)} + \frac{N}{2^l}\right) \tag{11}$$

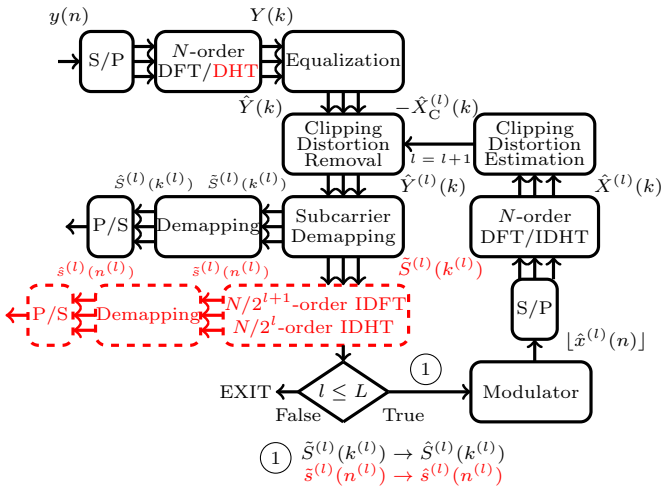

Figure 2: Receiver configuration for the layered approaches. For LACO-OFDM, after subcarrier demapping, the operations indicated in black boxes are performed. For FTP-LACO-OFDM and HTP-LACO-OFDM, after demapping, the operations indicated in dashed red boxes are additionally performed.

with $\tilde{n}^{(l)} = 0, 1, \cdots, N/2^l - 1$. For $l > 1$, $x^{(l)}(n) = x^{(l)} \mathrm{mod}\left(n, N/2^{l-1}\right)$, where $\mathrm{mod}(\cdot, N)$ is the modulo N operator. Because of the anti-symmetric property, $x^{(l)}(n)$ is clipped to zero without loss of information to yield:

$$\lfloor x^{(l)}(n) \rfloor = \begin{cases} x^{(l)}(n), & x^{(l)}(n) \geq 0 \\ 0, & x^{(l)}(n) < 0 \end{cases} = x_{\mathrm{D}}^{(l)}(n) + x_{\mathrm{C}}^{(l)}(n), \tag{12}$$

where $x_{\mathrm{D}}^{(l)}(n)$ and $x_{\mathrm{C}}^{(l)}(n)$ is the data-carrying signal and the clipping distortion for the lth layer, respectively. $x_{\mathrm{D}}^{(l)}(n)$ and $x_{\mathrm{C}}^{(l)}(n)$ can be evaluated as [23]:

$$x_{\mathrm{D}}^{(l)}(n) = \frac{1}{2} x^{(l)}(n), \tag{13}$$

and

$$x_{\mathrm{C}}^{(l)}(n) = \frac{1}{2} |x^{(l)}(n)|. \tag{14}$$

For lth layer, the subcarriers at indices $k_{\mathrm{D}}^{(l)} = 2^{l-1}(2k^{(l)} + 1)$ are data-carrying, while, the clipping distortion falls on indices $k_{\mathrm{C}}^{(l)} = 2^l k^{(l)}$. The clipped TD signals, $\lfloor x^{(l)}(n) \rfloor$ for $l = 1, 2, \cdots, L$ are combined as:

$$x(n) = \sum_{l=1}^{L} \lfloor x^{(l)}(n) \rfloor, \tag{15}$$

to yield the non-negative composite TD signal for transmission.

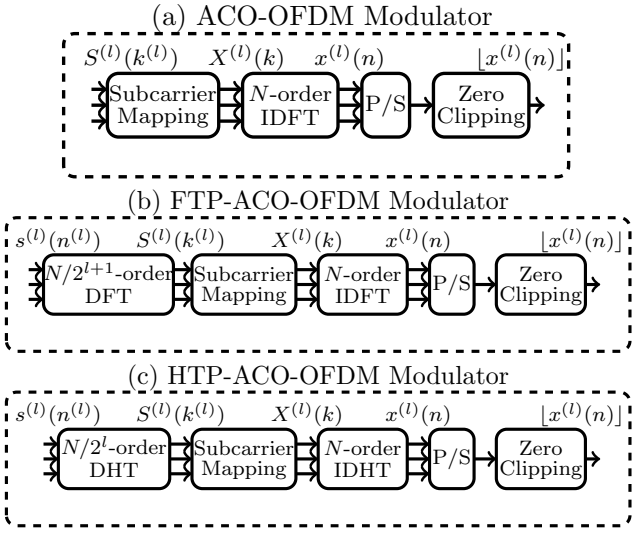

Figure 3: Modulator configurations for (a) ACO-OFDM, (b) FTP-ACO-OFDM and (c) HTP-ACO-OFDM.

3.1.2. Receiver

The transmitted data can be retrieved from (8). So, by incorporating (12) in (15) and using (8) we get:

$$\hat{Y}(k) = \sum_{l=1}^{L} \hat{X}_{\mathrm{D}}^{(l)}(k) + \sum_{l=1}^{L} \hat{X}_{\mathrm{C}}^{(l)}(k) + Z(k). \tag{16}$$

$\hat{X}_{\mathrm{D}}^{(l)}(k)$ and $\hat{X}_{\mathrm{C}}^{(l)}(k)$ are the FD counterparts of $x_{\mathrm{D}}^{(l)}(n)$ and $x_{\mathrm{C}}^{(l)}(n)$, respectively. Disseminated data on different layers is identified on a layer-to-layer basis. To correctly identify the transmitted data, the clipping distortion falling on the corresponding layer has to be removed, hence, $\hat{Y}^{(l)}(k) = \hat{Y}^{(l-1)}(k) - \hat{X}_{\mathrm{C}}^{(l)}(k)$. For layer 1, no clipping distortion falls on data-carrying subcarriers, hence, $\hat{X}_{\mathrm{C}}^{(1)}(k) = 0$, which results in $\hat{Y}^{(1)}(k) = \hat{Y}^{(0)}(k)$, where $\hat{Y}^{(0)}(k) = \hat{Y}(k)$. Transmitted data from $\hat{Y}^{(1)}(k)$ is recovered by choosing the relevant subcarriers; the indices of which can be determined by $k_{\mathrm{D}}^{(1)}$, hence, we have $\tilde{S}^{(1)}(k^{(1)}) = \hat{Y}^{(1)}(k_{\mathrm{D}}^{(1)})$. Decisions on $\tilde{S}^{(1)}(k^{(1)})$ are made according to:

$$\hat{S}^{(1)}(k^{(1)}) = \arg \min_{X_Q \in \boldsymbol{\mathcal{Q}}} \left\| 2\tilde{S}^{(1)}(k^{(1)}) - X_Q \right\|, \tag{17}$$

for $k^{(1)} = 0, 1, \cdots, N/4 - 1$.

For the subsequent layers, $l > 1$, clipping distortion altering the data-carrying subcarriers comes from $(l-1)$th layer. $\hat{X}_{\mathrm{C}}^{(l)}(k)$ is evaluated using $\hat{S}^{(l-1)}(k^{(l-1)})$ and deducted from $\hat{Y}^{(l)}(k)$, i.e., $\hat{Y}^{(l)}(k) = \hat{Y}^{(l-1)}(k) - \hat{X}_{\mathrm{C}}^{(l)}(k)$. The modulated subcarriers are retrieved as $\tilde{S}^{(l)}(k^{(l)}) = \hat{Y}^{(l)}(k_{\mathrm{D}}^{(l)})$ and transmitted data is identified as:

$$\hat{S}^{(l)}(k^{(l)}) = \arg \min_{X_Q \in \boldsymbol{\mathcal{Q}}} \left\| 2\tilde{S}^{(l)}(k^{(l)}) - X_Q \right\|. \tag{18}$$

3.2. FTP-LACO-OFDM

For FTP-LACO-OFDM, in addition to the operations needed for LACO-OFDM, FT precoding and FT decoding is needed at the transmitter and the receiver, respectively. This technique can be outlined as follows.

3.2.1. Transmitter

The serial incoming bits at the lth layer are mapped onto TD symbols, $s^{(l)}(n^{(l)}), n^{(l)} = 0, 1, \cdots, N/2^{l+1}-1$ drawn from $\boldsymbol{\mathcal{Q}}$ (rather than onto FD symbols as in LACO-OFDM). Thereafter, these TD symbols, $s^{(l)}(n^{(l)})$ are FT precoded via $N/2^{l+1}$-order DFT to yield:

$$S^{(l)}(k^{(l)}) = \text{DFT}\left[s^{(l)}(n^{(l)})\right], \tag{19}$$

where $k^{(l)} = n^{(l)}$. The subsequent operations required at the transmitter are the same as explained in (9)-(15).

3.2.2. Receiver

At the receiver, FT decoding is required before the detection of transmitted data. For each layer, after recovering $\tilde{S}^{(l)}(k^{(l)})$ as in LACO-OFDM, FT decoding is implemented via $N/2^{l+1}$-order IDFT to achieve:

$$\tilde{s}^{(l)}(n^{(l)}) = \text{IDFT}\left[\tilde{S}^{(l)}(k^{(l)})\right]. \tag{20}$$

Following which, the transmitted data on lth layer is detected as:

$$\hat{s}^{(l)}(n^{(l)}) = \arg \min_{X_Q \in \boldsymbol{\mathcal{Q}}} \left\| 2\tilde{s}^{(l)}(n^{(l)}) - X_Q \right\|. \tag{21}$$

Contrary to LACO-OFDM, where the estimate of clipping distortion for lth layer, $\hat{X}_{\text{C}}^{(l)}(k)$ is obtained via $\hat{S}^{(l-1)}(k^{(l-1)})$, in FTP-LACO-OFDM, $\hat{X}_{\text{C}}^{(l)}(k)$ is determined using $\hat{s}^{(l-1)}(n^{(l-1)})$.

3.3. HTP-LACO-OFDM

It is recalled that HTP-LACO-OFDM differs from both LACO-OFDM and FTP-LACO-OFDM. Some distinctions are: (i) the symbols are drawn from $\sqrt{M}$-ary PAM constellation rather than M-ary QAM constellation; (ii) HS is not required; and (iii) real-valued IDHT/DHT is adopted for multiplexing/demultiplexing rather than IDFT/DFT.

3.3.1. Transmitter

For layer l, the bits are mapped to $\sqrt{M}$-ary PAM TD symbols, $s^{(l)}(n^{(l)})$, $n^{(l)} = 0, 1, \cdots, N/2^{l}-1$, drawn from constellation set $\boldsymbol{\mathcal{P}} = \left\{\mathcal{P}_0, \mathcal{P}_1, \cdots, \mathcal{P}_{\sqrt{M}-1}\right\}$. Afterwards, $s^{(l)}(n^{(l)})$ are precoded using $N/2^{l}$-order DHT as:

$$S^{(l)}(k^{(l)}) = \text{DHT}\left[s^{(l)}(n^{(l)})\right], \tag{22}$$

for $k^{(l)} = n^{(l)}$. Subsequently, subcarrier mapping is performed by allocating $S^{(l)}(k^{(l)})$ to the N-length signal, $X^{(l)}(k), k = 0, 1, \cdots, N-1$ as:

$$X^{(l)}(k) = \begin{cases} S^{(l)}(k^{(l)}), & k = 2^{l-1}(2k^{(l)}+1) \\ 0, & \text{elsewhere} \end{cases}. \tag{23}$$

(23) differs from (9) because HS is excluded. Eventually, the subcarriers are multiplexed using N-order IDHT as:

$$x^{(l)}(n) = \text{IDHT}\left[X^{(l)}(k)\right], \tag{24}$$

for $n = 0, 1, \cdots, N-1$. $x^{(l)}(n)$ follows anti-symmetric characteristics, i.e.,

$$x^{(l)}(n^{(l)}) = -x^{(l)}\left(n^{(l)} + \frac{N}{2^l}\right). \tag{25}$$

$x^{(l)}(n)$ is clipped as in (12) to yield $\lfloor x^{(l)}(n) \rfloor$; from which $x(n)$ is attained as in (15). The data-carrying subcarriers on lth layer are identified by indices $k_{\text{D}}^{(l)} = 2^{l-1}(2k^{(l)}+1)$, while, the lth layer clipping distortion falls on subcarriers with indices, $k_{\text{C}}^{(l)} = 2^l k^{(l)}$.

3.3.2. Receiver

The equalized signal is the same as in (16); which, however, is obtained via a different equalization process. To determine the disseminated data, the clipping distortion landing on the corresponding layer has to be eliminated, so, $\hat{Y}^{(l)}(k) = \hat{Y}^{(l-1)}(k) - \hat{X}_{\text{C}}^{(l)}(k)$. For $l = 1$, no clipping distortion falls on the data-carrying subcarriers, i.e., $\hat{X}_{\text{C}}^{(1)}(k) = 0$, thus, $\hat{Y}^{(1)}(k) = \hat{Y}^{(0)}(k)$ with $\hat{Y}^{(0)}(k) = \hat{Y}(k)$. For the following layers, $l > 1$, $\hat{X}_{\text{C}}^{(l)}(k)$ is obtained via $\hat{s}^{(l-1)}(n^{(l-1)})$ and is deducted from $\hat{Y}^{(l)}(k)$. For each layer, the subcarriers are determined as $\tilde{S}^{(l)}(k^{(l)}) = \hat{Y}^{(l)}(k_{\text{D}}^{(l)})$. Afterwards, HT decoding is performed using $N/2^l$-order IDHT, which yields:

$$\tilde{s}^{(l)}(n^{(l)}) = \text{IDHT}\left[\tilde{S}^{(l)}(k^{(l)})\right]. \tag{26}$$

Lastly, the transmitted data is identified as:

$$\hat{s}^{(l)}(n^{(l)}) = \arg \min_{X_P \in \boldsymbol{\mathcal{P}}} \left\| 2\tilde{s}^{(l)}(n^{(l)}) - X_P \right\|. \tag{27}$$

4. Performance Analysis and Discussions

4.1. Statistical Properties

The TD signal of LACO-OFDM at different layers, $x^{(l)}(n)$ manifests Gaussian distribution [9]. Graphical interpretation for the probability density functions (pdfs) of $x^{(l)}(n)$ considering $L = 3$, $M = 4$ and $N = 2048$ is presented in Fig. 4. For transmission, these TD signals would be clipped and combined to attain a composite TD signal, $x(n)$. It is easy to comprehend that the distribution of $x(n)$ would be truncated Gaussain function with the negative fraction entirely clipped

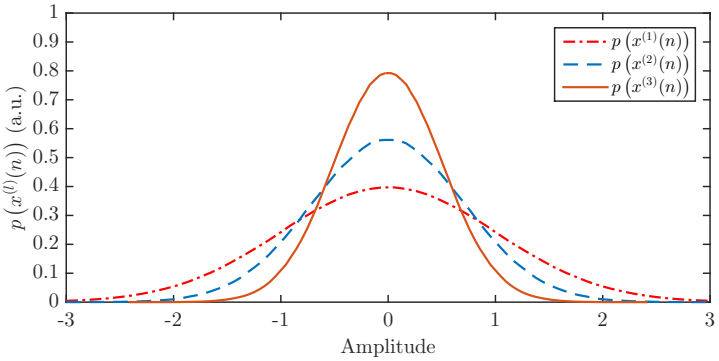

Figure 4: Probability density function for unclipped TD LACO-OFDM signals.

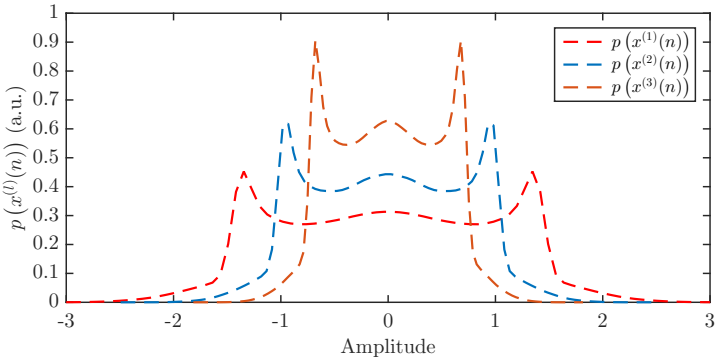

Figure 5: Probability density function for unclipped TD FTP-LACO-OFDM signals.

[9]. Moreover, if the composite TD signals follow truncated Gaussian distribution, the assessment of parameters, such as, electrical and optical powers of $x(n)$ is mathematically feasible [9].

On the other hand, evaluation of closed-form expressions for the pdfs of composite TD signals for precoded layered approaches is cumbersome. Graphical depiction of the expected pdfs for TD signals, $x^{(l)}(n)$ for 4-QAM FTP-LACO-OFDM and 2-PAM HTP-LACO-OFDM using $L = 3$, $M = 4$ and $N = 2048$ is presented in Fig. 5 and Fig. 6, respectively. It may be noticed that substantial mathematical modeling is required to characterize such distributions. Even then, with a variation in alphabet cardinality, M or $\sqrt{M}$, the distributions would change altogether. Hence, for every modulation alphabet, a unique distribution has to be evaluated; which is mathematically intractable.

Furthermore, if we interpret the estimated pdfs of the composite TD signal, $x(n)$ for precoded and non-precoded LACO-OFDM as shown in Fig. 7 (obtained using $N = 2048, L = 3$ and $M = 4$), it is obvious that the distributions of FTP-LACO-OFDM and HTP-LACO-OFDM does not adhere to any known distributions. As a consequence of these unknown distributions of composite TD signals, $x(n)$ for FTP-LACO-OFDM and HTP-LACO-OFDM is that the computation of closed-

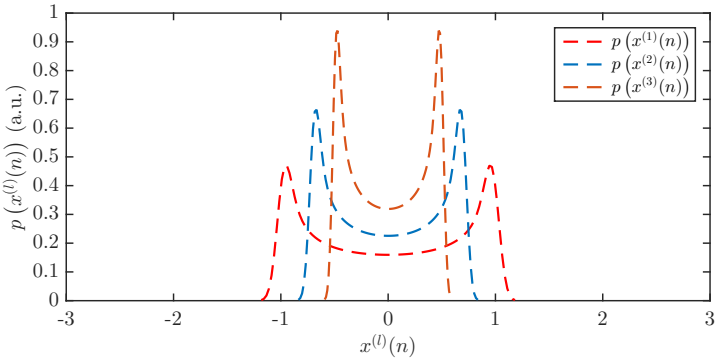

Figure 6: Probability density function for unclipped TD HTP-LACO-OFDM signals.

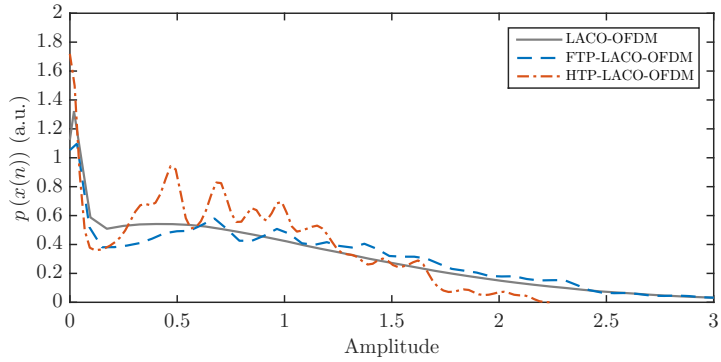

Figure 7: Probability density function for composite TD signals for LACO-OFDM, FTP-LACO-OFDM and HTP-LACO-OFDM. Note that, the spikes in the pdfs at signal amplitude corresponding to zero is due to zero level clipping.

form expressions for electrical and optical powers is not possible. Regardless, mathematically, the average electrical power for the composite TD signal considering L independent layers (for all the approaches) is given as [10, 11]:

$$\begin{aligned} P_{(\text{elec},\cdot)} &= E\left(|x(n)|^2\right) = E\left(\left\{\sum_{l=1}^{L}\lfloor x^{(l)}(n)\rfloor\right\}^2\right) \\ &= \sum_{l=1}^{L} E\left(\lfloor x^{(l)}(n)\rfloor^2\right) \\ &\quad + \sum_{l\neq l_1}^{L} E\left(\lfloor x^{(l)}(n)\rfloor\right) E\left(\lfloor x^{(l_1)}(n)\rfloor\right). \end{aligned} \tag{28}$$

Similarly, the average optical power of the composite TD signal with L independent layers for

the layered approaches can be calculated as [10, 11]:

$$P_{(\text{opt},\cdot)} = E\left(|x(n)|\right) = E\left(\sum_{l=1}^{L} \lfloor x^{(l)}(n) \rfloor\right). \tag{29}$$

(28) and (29) entail that a closed-form expressions for the average electrical and average optical power can be computed only if the distribution of clipped TD signal at each layer, i.e., $\lfloor x^{(l)}(n) \rfloor$ is known, which, unlike LACO-OFDM, is not the case with FTP-LACO-OFDM and HTP-LACO-OFDM. Therefore, in the sequel, we have relied on the simulation values for these parameters.

4.2. Layering Attenuation

Recognizing same modulation alphabet cardianlity for all the layers, we adopt a fair power allocation approach, wherein, the average electrical power administered to a layer conforms to the number of data-carrying subcarriers. So, the average electrical power of the lth layer, $P^{(l)}_{(\text{elec},\cdot)}$ is half of $(l-1)$th layer, $P^{(l-1)}_{(\text{elec},\cdot)}$ yielding:

$$P^{(l)}_{(\text{elec},\cdot)} = \frac{1}{2} P^{(l-1)}_{(\text{elec},\cdot)}, \tag{30}$$

for $l = 2, 3, \cdots, L$. For M-ary QAM based LACO-OFDM and FTP-LACO-OFDM, $P^{(1)}_{(\text{elec,LACO})} = P^{(1)}_{(\text{elec,FTP})} = E\left(\lfloor x^{(1)}(n) \rfloor^2\right) = \sigma_x^2/2 = (M-1)/6$, while, for HTP-LACO-OFDM employing $\sqrt{M}$-ary PAM alphabets, $P^{(1)}_{(\text{elec,HTP})} = E\left(\lfloor x^{(1)}(n) \rfloor^2\right) = \sigma_x^2/2 = (M-1)/12$. σ_x^2 is the variance of the TD signal for the first layer before clipping which is calculated as $E\left(|x^{(1)}(n)|^2\right)$. These relations are evaluated knowing that the average symbol energy of M-ary QAM and $\sqrt{M}$-ary PAM modulation alphabet is $2(M-1)/3$ and $(M-1)/3$.

Moreover, the average number of bits encoded in layered variants with L layers are:

$$\Theta = 2 - \frac{1}{2^{L-1}}, \tag{31}$$

times higher than the bits encoded in conventional counterparts [11]. Because of layered structure, the layered variants emanate an attenuation, called *layering attenuation* compared to their traditional counterparts. Using (30) and (31), layering attenuation is computed as [10, 11]:

$$\alpha_{(\cdot)}(L) = 10 \log_{10} \left\{ \frac{1}{\Theta} \left(\frac{P_{(\text{elec},\cdot)}}{P^{(1)}_{(\text{elec},\cdot)}} \right) \right\} \quad \text{(dB)}, \tag{32}$$

where $P_{(\text{elec},\cdot)}$ is the electrical power of the composite TD signal, and $P^{(1)}_{(\text{elec},\cdot)}$ is the electrical power of the first layer. (32) signifies that the electrical SNR to reach a given BER increase by a factor of $\alpha_{(\cdot)}(L)$ when layered variants are chosen instead of the traditional counterparts for the same modulation alphabet size. However, for layered variants, the SE would be augmented compared to traditional counterparts.

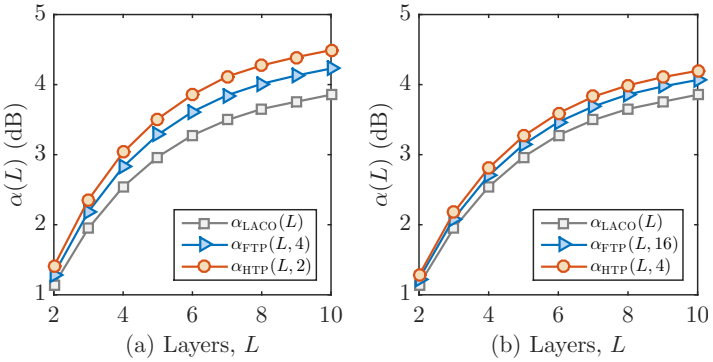

Figure 8: Layering attenuation as a function of number of layers, L: (a) $M = 4$; (b) $M = 16$.

The layereing attenuation, $\alpha_{(.)}(L)$ for LACO-OFDM only depends on the number of layers, L because the distribution of composite TD signal is the same irrespective of modulation alphabet cardinality. Whereas, for FTP-LACO-OFDM and HTP-LACO-OFDM, $\alpha_{(.)}(L)$ depends on both the number of layers, L, and modulation alphabet size, M or $\sqrt{M}$; because the pdfs of composite TD signal change with a change in modulation alphabet. So, $\alpha_{(.)}(L)$ can be explicitly addressed as $\alpha_{\text{LACO}}(L)$, $\alpha_{\text{FTP}}(L, M)$ and $\alpha_{\text{HTP}}(L, \sqrt{M})$. Fig. 8 (a) and Fig. 8 (b) show the simulated layering attenuation $\alpha_{(.)}(L)$ as a function of number of layers, L, for LACO-OFDM, FTP-LACO-OFDM and HTP-LACO-OFDM using $M = 4$ and $M = 16$, respectively. The number of subcarriers used for simulation are $N = 2048$. The simulated results show that:

$$\alpha_{\text{LACO}}(L) < \alpha_{\text{FTP}}(L, M) < \alpha_{\text{HTP}}(L, \sqrt{M}). \tag{33}$$

It can be established that LACO-OFDM incurs a lower layering attenuation compared to FTP-LACO-OFDM and HTP-LACO-OFDM for both $M = \{4, 16\}$. Other distinctive trends which can be followed from Fig. 8 are: (i) $\alpha_{(.)}(L)$ is an increasing function of number of layers, L; and (ii) $\alpha_{\text{FTP}}(L, M)$ and $\alpha_{\text{HTP}}(L, \sqrt{M})$ diminishes with the increase in modulation alphabet cardinality.

4.3. Spectral Efficiency

SE of M-ary QAM based LACO-OFDM and $\sqrt{M}$-ary PAM based HTP-LACO-OFDM is

$$\eta_{\text{LACO}}(L) = \frac{\log_2(M) \sum_{l=1}^{L} (N/2^{l+1})}{(N + N_{\text{CP}})} \quad \text{(bits/s/Hz)}, \tag{34}$$

and

$$\eta_{\text{HTP}}(L) = \frac{\log_2(\sqrt{M}) \sum_{l=1}^{L} (N/2^{l})}{(N + N_{\text{CP}})} \quad \text{(bits/s/Hz)}, \tag{35}$$

respectively, where N_{CP} is the length of CP. The SE of FTP-LACO-OFDM is same as that of LACO-OFDM, i.e., $\eta_{\text{FTP}}(L) = \eta_{\text{LACO}}(L)$ (for same N_{CP}).

The aim of the layered approaches is to augment the spectral efficiencies of ACO-OFDM, FTP-ACO-OFDM and HTP-ACO-OFDM towards that of DCO-OFDM, η_{DCO}, i.e., $\lim_{L\to\infty}\eta_{(\cdot)}(L) = \eta_{\mathrm{DCO}}$, i.e., the SE of layered approaches increases with an increase in L [8, 11], e.g., by increasing $L = 2$ to $L = 5$, $\eta_{(\cdot)}(L)$ increases from 75% to 96.9% of η_{DCO}. Moreover, theoretically η_{DCO} can be achieved for $L \to \infty$. Regardless, it should be realized that maximum number of layers that can be modulated with N subcarriers are $L \leq \log_2(N) - 1$ for LACO-OFDM and FTP-LACO-OFDM. On the other hand, for HTP-LACO-OFDM, $L \leq \log_2(N)$ layers can be modulated with N subcarriers. It may be noticed that maximum number of modulated layers for HTP-LACO-OFDM are higher compared to LACO-OFDM and FTP-LACO-OFDM because HS is not required.

4.4. Electrical-to-Optical Power Conversion Efficiency

The electrical-to-optical power conversion efficiency measures how much electrical power is converted into optical power (at the LED) and can be evaluated as:

$$\alpha^{\mathrm{EO}}_{(\cdot)}(L) = 10\log_{10}\left\{\frac{P_{(\mathrm{elec},\cdot)}}{P_{(\mathrm{opt},\cdot)}}\right\} \quad (\mathrm{dB}), \tag{36}$$

where $P_{(\mathrm{opt},\cdot)}$ is the average optical power. For an impartial comparison, $P_{(\mathrm{opt},\cdot)}$ is scaled to unity to evaluate $\alpha^{\mathrm{EO}}_{(\cdot)}(L)$ [28]. A high value of $\alpha^{\mathrm{EO}}_{(\cdot)}(L)$ signify better electrical-to-optical power conversion efficiency. The simulation results for expected efficiencies as a function of the number of layers, L, are presented in Fig. 9; which are obtained using $N = 2048$. It can be observed that $\alpha^{\mathrm{EO}}_{(\cdot)}(L)$ for LACO-OFDM solely depends on the number of layers, L, whereas, for precoded counterparts, $\alpha^{\mathrm{EO}}_{(\cdot)}(L)$ is bounded by L and the modulation alphabet size, M or $\sqrt{M}$. Accordingly, for clarity of exposition, we can write $\alpha^{\mathrm{EO}}_{\mathrm{LACO}}(L)$, $\alpha^{\mathrm{EO}}_{\mathrm{FTP}}(L, M)$ and $\alpha^{\mathrm{EO}}_{\mathrm{HTP}}(L, \sqrt{M})$. As aforementioned, this dependency on modulation alphabet cardinality for precoded approaches is due to change in the pdfs of composite TD signals for different modulation alphabets. Fig. 9 also reveals that

$$\alpha^{\mathrm{EO}}_{\mathrm{LACO}}(L) > \alpha^{\mathrm{EO}}_{\mathrm{FTP}}(L, M) > \alpha^{\mathrm{EO}}_{\mathrm{HTP}}(L, \sqrt{M}). \tag{37}$$

Other noteworthy trends that can be identified from Fig. 9 are: (i) $\alpha^{\mathrm{EO}}_{(\cdot)}(L)$ diminishes with an increase in the number of layers, L; and (ii) $\alpha^{\mathrm{EO}}_{\mathrm{FTP}}(L, M)$ and $\alpha^{\mathrm{EO}}_{\mathrm{HTP}}(L, \sqrt{M})$ increase with an increase in modulation alphabet cardinality.

4.5. Bit Error Rate Performance

In this section, the BER performances of LACO-OFDM, FTP-LACO-OFDM and HTP-LACO-OFDM have been assessed considering: (i) an AWGN channel, (ii) a classical indoor VLC channel in combination with bandwidth limitation of LED in combination with its driver, and (iii) non-linear distortions. The electrical and optical SNR per bit for the system, $E_{\mathrm{b}_{(\mathrm{elec})}}/N_0$ and $E_{\mathrm{b}_{(\mathrm{opt})}}/N_0$, for LACO-OFDM and FTP-LACO-OFDM is defined as:

$$\frac{E_{\mathrm{b}_{(\mathrm{elec})}}}{N_0} = \frac{P_{(\mathrm{elec,LACO/FTP})}}{B\eta_{\mathrm{LACO/FTP}}(L)N_0}, \tag{38}$$

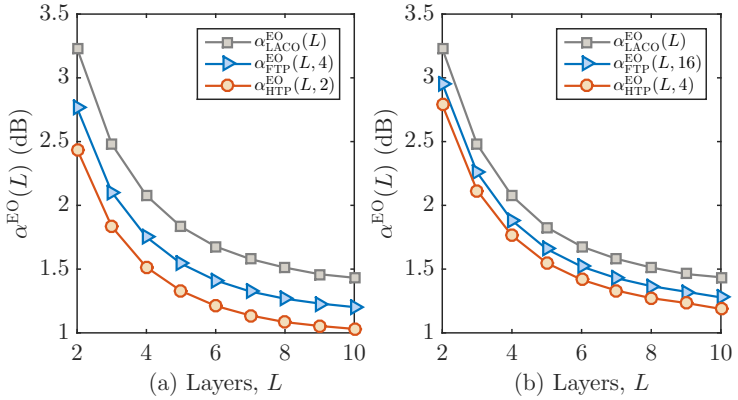

Figure 9: Optical-to-electrical conversion gain for LACO-OFDM: (a) $M = 4$; (b) $M = 16$.

and

$$\frac{E_{\mathrm{b}_{(\mathrm{opt})}}}{N_0} = \frac{P_{(\mathrm{opt,LACO/FTP})}}{B\eta_{\mathrm{LACO/FTP}}(L)N_0}, \tag{39}$$

respectively, where B is the mono-lateral communication bandwidth. For HTP-LACO-OFDM, $E_{\mathrm{b}_{(\mathrm{elec})}}/N_0$ and $E_{\mathrm{b}_{(\mathrm{opt})}}/N_0$ are obtained as:

$$\frac{E_{\mathrm{b}_{(\mathrm{elec})}}}{N_0} = \frac{P_{(\mathrm{elec,HTP})}}{2B\eta_{\mathrm{HTP}}(L)N_0}, \tag{40}$$

and

$$\frac{E_{\mathrm{b}_{(\mathrm{opt})}}}{N_0} = \frac{P_{(\mathrm{opt,HTP})}}{2B\eta_{\mathrm{HTP}}(L)N_0}. \tag{41}$$

Multiplication by 2 in the denominator of (40) and (41) is mandatory because HTP-LACO-OFDM employs $\sqrt{M}$-ary PAM alphabets rather than M-ary QAM alphabets. Using (38), (39), (40) and (41), a relationship between $E_{\mathrm{b}_{(\mathrm{elec})}}/N_0$ and $E_{\mathrm{b}_{(\mathrm{opt})}}/N_0$ can be appraised as:

$$\alpha^{\mathrm{EO}}_{(\cdot)}(L)\frac{E_{\mathrm{b}_{(\mathrm{opt})}}}{N_0} = \frac{E_{\mathrm{b}_{(\mathrm{elec})}}}{N_0}. \tag{42}$$

(42) implies that for any $E_{\mathrm{b}_{(\mathrm{elec})}}/N_0$, the corresponding $E_{\mathrm{b}_{(\mathrm{opt})}}/N_0$ can be obtained by scaling $E_{\mathrm{b}_{(\mathrm{elec})}}/N_0$ by $\alpha^{\mathrm{EO}}_{(\cdot)}(L)$.

The BER performances of LACO-OFDM, FTP-LACO-OFDM and HTP-LACO-OFDM are assessed in an AWGN for $\eta_{(\cdot)}(L) \approx \{2, 3, 4, 5\}$ bits/s/Hz, and in time dispersive channels for $\eta_{(\cdot)}(L) \approx \{1, 2\}$ bits/s/Hz. Considering non-linear distortions, the BER performances are appraised for $\eta_{(\cdot)(L)} \approx 2$ bits/s/Hz. We use $L = 5$ and the results are averaged over 2000 independent realizations with $N = 2048$. For the time dispersive channel, the dispersions are characterized by multipath VLC propagation and bandwidth limitation of LED in combination with its optimized driver. Thus, the overall channel impulse response (CIR), $h(t)$ in discrete representation can be

given as:

$$h(n) = h_{\text{LED}}(n) \otimes h_{\text{chan}}(n), \tag{43}$$

where $h_{\text{LED}}(n)$ is the impulse response of the LED, and $h_{\text{chan}}(n)$ are multipath VLC channel coefficients. $h_{\text{LED}}(n)$ is modeled as a Gaussian low-pass filter with transfer function:

$$H_{\text{LED}}(f) = \exp\left[-\ln(2)\left(\frac{f}{f_{\text{3dB}}}\right)^2\right], \tag{44}$$

where the 3 dB optical cut-off frequency of the LED with an optimized driver, f_{3dB} is set at 150 MHz [23, 29]. $h_{\text{chan}}(n)$ is obtained via recursive ray tracing algorithm in typical indoor VLC scenarios [30]. The CIR is obtained via the same configuration as presented in [30] and a sampling time of 1 ns. The bandwidth (BW) of transmit signal (in case of time dispersive channel) is set at 200 MHz, thus, culminating a noticeable impact of bandwidth limitation of the LED/LED driver combo.

4.5.1. BER Performance in AWGN Channel

The BER performances of the layered approaches as a function of $E_{\text{b}_{(\text{elec})}}/N_0$ are presented in Fig. 10. It is ascertained that BER performance of LACO-OFDM is better than FTP-LACO-OFDM and HTP-LACO-OFDM because it encounters a lesser layering attenuation from the superimposed structure. Additionally, since, $\alpha_{\text{HTP}}(L, \sqrt{M})$ has the largest value among the layered techniques, therefore, the increment in $E_{\text{b}_{(\text{elec})}}/N_0$ to attain a given BER is also highest. The difference between the required $E_{\text{b}_{(\text{elec})}}/N_0$ for FTP-LACO-OFDM and HTP-LACO-OFDM compared to LACO-OFDM would be the difference between the two layering attenuation values, i.e.,

$$\beta^{(\text{elec})}_{\text{FTP}}(L, M) = \frac{\alpha_{\text{FTP}}(L, M)}{\alpha_{\text{LACO}}(L)} \quad \text{(dB)}, \tag{45}$$

and

$$\beta^{(\text{elec})}_{\text{HTP}}(L, \sqrt{M}) = \frac{\alpha_{\text{HTP}}(L, \sqrt{M})}{\alpha_{\text{LACO}}(L)} \quad \text{(dB)}, \tag{46}$$

respectively. Here, $\beta^{(\text{elec})}_{\text{HTP}}(L, \sqrt{M}) > \beta^{(\text{elec})}_{\text{FTP}}(L, M)$ because $\alpha_{\text{HTP}}(L, \sqrt{M}) > \alpha_{\text{FTP}}(L, M)$.

We now proceed to assessing the BER performances of these layered techniques considering $E_{\text{b}_{(\text{opt})}}/N_0$. The results are portrayed in Fig. 11. Now, along with $\alpha_{(\cdot)}(L)$, another parameter that influences the BER performance is $\alpha^{\text{EO}}_{(\cdot)}(L)$. It may be noticed that LACO-OFDM requires lower $E_{\text{b}_{(\text{opt})}}/N_0$ because the layering attenuation is less and the electrical-to-optical power conversion efficiency is high compared to other counterparts. On the other hand, the performance of HTP-LACO-OFDM is worst because of higher layering attenuation and diminished electrical-to-optical power conversion efficiency. The performance of FTP-LACO-OFDM is better than HTP-LACO-OFDM, but is worse than LACO-OFDM. The gain in $E_{\text{b}_{(\text{opt})}}/N_0$ for LACO-OFDM over FTP-LACO-OFDM and HTP-LACO-OFDM can be evaluated as:

$$\beta^{(\text{opt})}_{\text{FTP}}(L, M) = \beta^{(\text{elec})}_{\text{FTP}}(L, M) + \frac{\alpha^{\text{EO}}_{\text{LACO}}(L)}{\alpha^{\text{EO}}_{\text{FTP}}(L, M)} \quad \text{(dB)}, \tag{47}$$

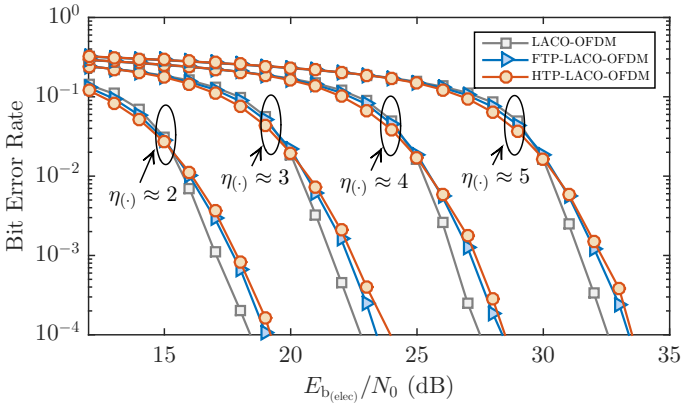

Figure 10: BER comparison of LACO-OFDM, FTP-LACO-OFDM and HTP-LACO-OFDM as a function of $E_{b_{(elec)}}/N_0$ considering an AWGN channel, $\eta_{(\cdot)} \approx \{2, 3, 4, 5\}$ bits/s/Hz and $L = 5$.

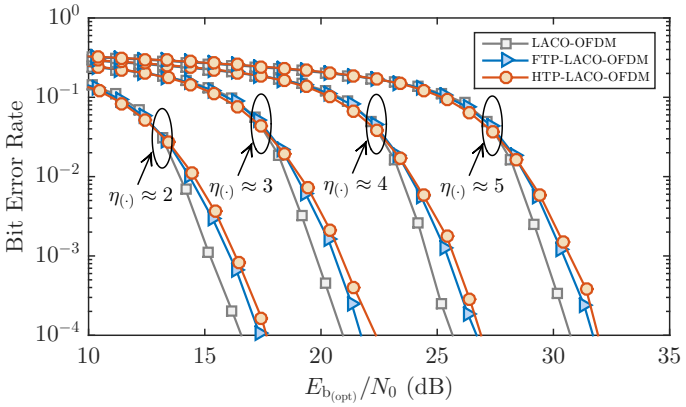

Figure 11: BER comparison of LACO-OFDM, FTP-LACO-OFDM and HTP-LACO-OFDM as a function of $E_{b_{(opt)}}/N_0$ considering an AWGN channel, $\eta_{(\cdot)} \approx \{2, 3, 4, 5\}$ bits/s/Hz and $L = 5$.

and

$$\beta_{\text{HTP}}^{(\text{opt})}(L, \sqrt{M}) = \beta_{\text{HTP}}^{(\text{elec})}(L, \sqrt{M}) + \frac{\alpha_{\text{LACO}}^{\text{EO}}(L)}{\alpha_{\text{HTP}}^{\text{EO}}(L, \sqrt{M})} \quad \text{(dB)}, \tag{48}$$

respectively. $\beta_{\text{HTP}}^{(\text{opt})}(L, \sqrt{M}) > \beta_{\text{FTP}}^{(\text{opt})}(L, M)$ because $\beta_{\text{HTP}}^{(\text{elec})}(L, \sqrt{M}) > \beta_{\text{FTP}}^{(\text{elec})}(L, M)$ and $\alpha_{\text{HTP}}^{\text{EO}}(L, \sqrt{M}) < \alpha_{\text{FTP}}^{\text{EO}}(L, M)$.

4.5.2. BER Performance in Time Dispersive Channel

In a time dispersive channel, the noise variance for LACO-OFDM post equalization is $N_0/|H(k)|^2$ (for ZF equalization), whilst, for the FTP-LACO-OFDM and HTP-LACO-OFDM, there is an averaging effect on the noise variance because of the decoder, hence, the noise variance is $1/N \sum_{k=0}^{N-1} N_0/|H(k)|^2$ [19]. Consequently, in precoded approaches, all the subcarriers encounter the same averaged SNR, which is not the case with LACO-OFDM, where the SNR varies per subcarrier; introducing a BER

degradation [19]. So, in case of time dispersive channel, the gain in $E_{\mathrm{b}_{(\mathrm{elec})}}/N_0$ for FTP-LACO-OFDM and HTP-LACO-OFDM over LACO-OFDM is attained as:

$$\hat{\beta}^{(\mathrm{elec})}_{\mathrm{FTP}}(L,M) = 3 - \beta^{(\mathrm{elec})}_{\mathrm{FTP}}(L,M) \quad \text{(dB)}, \tag{49}$$

and

$$\hat{\beta}^{(\mathrm{elec})}_{\mathrm{HTP}}(L,\sqrt{M}) = 3 - \beta^{(\mathrm{elec})}_{\mathrm{HTP}}(L,\sqrt{M}) \quad \text{(dB)}, \tag{50}$$

respectively, where $\hat{\beta}^{(\mathrm{elec})}_{\mathrm{FTP}}(L,M) > \hat{\beta}^{(\mathrm{elec})}_{\mathrm{HTP}}(L,\sqrt{M})$, since, $\beta^{(\mathrm{elec})}_{\mathrm{FTP}}(L,M) < \beta^{(\mathrm{elec})}_{\mathrm{HTP}}(L,\sqrt{M})$. Similarly, in terms of $E_{\mathrm{b}_{(\mathrm{opt})}}/N_0$, a gain of

$$\hat{\beta}^{(\mathrm{opt})}_{\mathrm{FTP}}(L,M) = 3 - \beta^{(\mathrm{opt})}_{\mathrm{FTP}}(L,M) \quad \text{(dB)}, \tag{51}$$

and

$$\hat{\beta}^{(\mathrm{opt})}_{\mathrm{HTP}}(L,\sqrt{M}) = 3 - \beta^{(\mathrm{opt})}_{\mathrm{HTP}}(L,\sqrt{M}) \quad \text{(dB)}, \tag{52}$$

would be observed for FTP-LACO-OFDM and HTP-LACO-OFDM, respectively over LACO-OFDM. Here, $\hat{\beta}^{(\mathrm{opt})}_{\mathrm{FTP}}(L,M) > \hat{\beta}^{(\mathrm{opt})}_{\mathrm{HTP}}(L,\sqrt{M})$, since, $\beta^{(\mathrm{opt})}_{\mathrm{FTP}}(L,M) < \beta^{(\mathrm{opt})}_{\mathrm{HTP}}(L,\sqrt{M})$.

Fig. 12 presents the BER performances of LACO-OFDM, FTP-LACO-OFDM and HTP-LACO-OFDM versus $E_{\mathrm{b}_{(\mathrm{elec})}}/N_0$ in time dispersive channel which demonstrates that FTP-LACO-OFDM and HTP-LACO-OFDM exhibit superior performance compared to LACO-OFDM. This corroborates the conclusions in the preceding paragraph where it is described that FTP-LACO-OFDM and HTP-LACO-OFDM would manifest an improvement of $\hat{\beta}^{(\mathrm{elec})}_{\mathrm{FTP}}(L,M)$ dB and $\hat{\beta}^{(\mathrm{elec})}_{\mathrm{HTP}}(L,\sqrt{M})$ dB, respectively, over LACO-OFDM. This improvement in performance for the precoded approaches is because all the subcarriers for the precoded approaches have the same SNR; which is not the case with LACO-OFDM. Furthermore, in terms of BER performance as a function of $E_{\mathrm{b}_{(\mathrm{opt})}}/N_0$ illustrated in Fig. 13, an identical trend is observed, where, the performances of precoded LACO-OFDM techniques are better than traditional LACO-OFDM. An improvement of almost $\hat{\beta}^{(\mathrm{opt})}_{\mathrm{FTP}}(5,4) \approx 2.39$ dB and $\hat{\beta}^{(\mathrm{opt})}_{\mathrm{FTP}}(5,16) \approx 2.65$ dB for $\eta_{(\cdot)} \approx 1$ bits/s/Hz and $\hat{\beta}^{(\mathrm{opt})}_{\mathrm{HTP}}(5,2) \approx 2$ dB and $\hat{\beta}^{(\mathrm{opt})}_{\mathrm{HTP}}(5,4) \approx 2.42$ dB for $\eta_{(\cdot)} \approx 2$ bits/s/Hz is recognized in terms of $E_{\mathrm{b}_{(\mathrm{opt})}}/N_0$ for FTP-LACO-OFDM and HTP-LACO-OFDM over LACO-OFDM.

4.5.3. BER Performance Considering non-linear Distortions

In practical scenarios, the transmit signal may experience non-linear distortions, such as, upper level (UL) clipping, either due to saturation of the light source or clipping from DAC [11]. This UL clipping may drastically impact the BER performance. However, it is foreseen that if signal manifests low PAPR, clipping distortion can be marginal, while the modulation efficiency is preserved. To assimilate the UL clipping impact, we define clipping ratio as:

$$\tau = 10\log_{10}\left(\frac{\gamma^2}{P_{(\mathrm{elec},\cdot)}}\right) \quad \text{(dB)}, \tag{53}$$

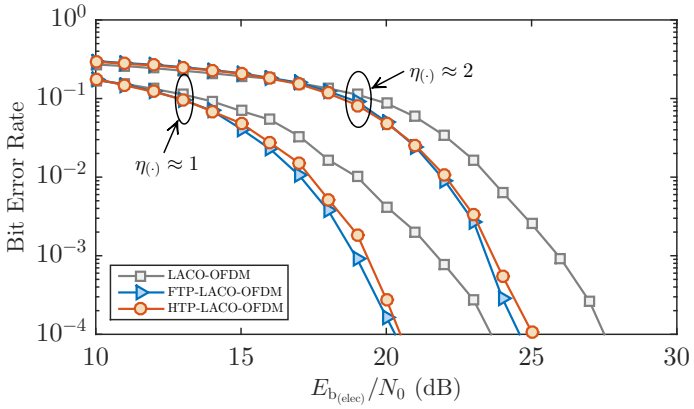

Figure 12: BER comparison of LACO-OFDM, FTP-LACO-OFDM and HTP-LACO-OFDM as a function of $E_{b_{(elec)}}/N_0$ considering a time dispersive channel, $\eta_{(\cdot)} \approx \{1, 2\}$ bits/s/Hz and $L = 5$.

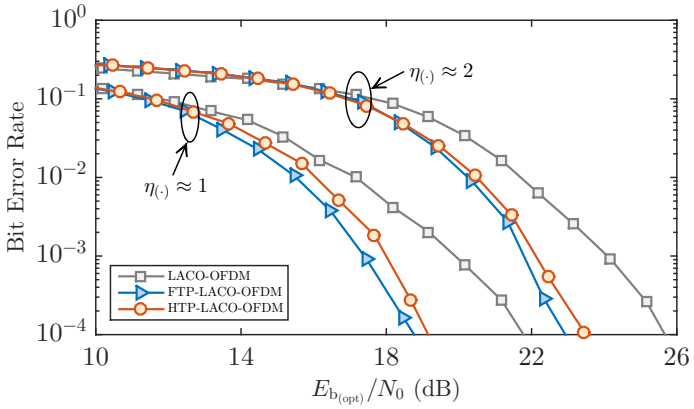

Figure 13: BER comparison of LACO-OFDM, FTP-LACO-OFDM and HTP-LACO-OFDM as a function of $E_{b_{(opt)}}/N_0$ considering a time dispersive channel, $\eta_{(\cdot)} \approx \{1, 2\}$ bits/s/Hz and $L = 5$.

where γ is the clipping threshold. Fig. 14(a)-(d) portray the BER performance of LACO-OFDM, FTP-LACO-OFDM and HTP-LACO-OFDM for $\eta_{(\cdot)} \approx 2$ considering $\tau = \{5, 7, 9, 11\}$ dB. It is discerned that FTP-LACO-OFDM and HTP-LACO-OFDM outperform LACO-OFDM for smaller values of τ because of lower PAPR (Fig. 14(a)-(b)). However, as τ increases, the performance of all schemes converge to that in AWGN channel because of a reduction in clipping distortion (Fig. 14(d)). For smaller values of τ, the performance of HTP-LACO-OFDM is always the best.

4.6. PAPR Analysis

To validate the aforementioned interpretations, PAPR of the considered modulation techniques have been evaluated. PAPR is a measure of deviation of the signal around its mean. Mathematically,

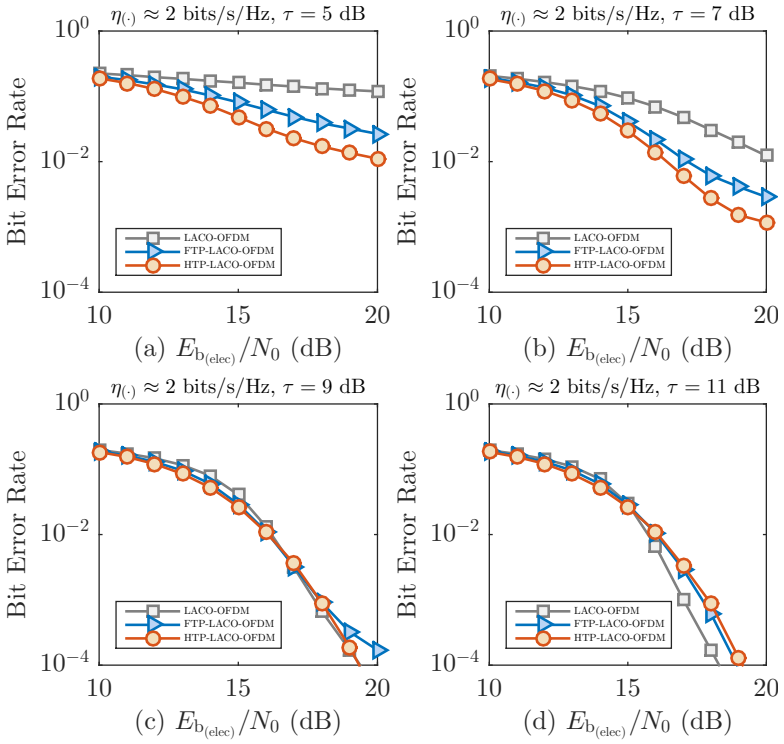

Figure 14: BER comparison of LACO-OFDM, FTP-LACO-OFDM and HTP-LACO-OFDM considering AWGN, UL clipping and $\eta_{(\cdot)} \approx 2$ bits/s/Hz with $L = 5$.

for an arbitrary N-length signal, $r(n)$, PAPR is expressed as:

$$\text{PAPR} = \lambda \triangleq \frac{\max\limits_{0 \leq n \leq N-1} \left(|r(n)|^2 \right)}{E\left(|r(n)|^2 \right)}. \tag{54}$$

PAPR is assessed using complementary cumulative distribution function (CCDF) which is the probability that the signal PAPR will transcend a threshold, PAPR_ϵ, i.e., CCDF = Prob(PAPR > PAPR_ϵ). For comparison, a criterion $\lambda_{(\cdot)}^{\max}$ is introduced which appraises the maximum PAPR at CCDF = 0.1. It is asserted that the PAPR of LACO-OFDM depends on the number of layers, L, number of subcarriers, N, and is autonomous of the modulation alphabet cardinality. However, for FTP-LACO-OFDM and HTP-LACO-OFDM, the PAPR also depends on the size of modulation alphabets. Hence, we can clearly define $\lambda_{(\cdot)}^{\max}$ as $\lambda_{\text{LACO}}^{\max}(L, N)$, $\lambda_{\text{FTP}}^{\max}(L, N, M)$ and $\lambda_{\text{HTP}}^{\max}(L, N, \sqrt{M})$. PAPR behavior of LACO-OFDM, FTP-LACO-OFDM and HTP-LACO-OFDM as a function of number of layers, L, is plotted in Fig. 15(a) for $M = 4$ and Fig. 15(b) for $M = 16$ and employing $N = 2048$. It is recognized that for $M = 4$ and $L = 5$, FTP-LACO-OFDM and HTP-LACO-OFDM manifest approximately 3.4 dB and 1.4 dB lesser PAPR than LACO-OFDM. For $M = 16$, the gain

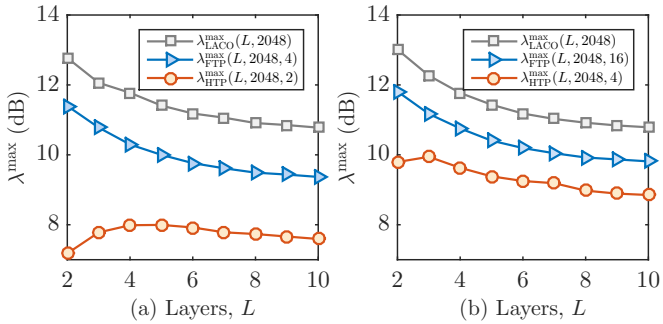

Figure 15: PAPR at CCDF = 0.1 as a function of L for LACO-OFDM, FTP-LACO-OFDM and HTP-LACO-OFDM: (a) $M = 4$; (b) $M = 16$.

is lowered to approximately 2 dB and 1 dB. Certainly, it is noticeable that HTP-LACO-OFDM exhibits the least PAPR among all the approaches. Thus, we have:

$$\lambda^{\max}_{\text{HTP}}(L, N, \sqrt{M}) < \lambda^{\max}_{\text{FTP}}(L, N, M) < \lambda^{\max}_{\text{LACO}}(L, N). \tag{55}$$

Fig. 16 illustrates the PAPR performance at CCDF = 0.1 for LACO-OFDM, FTP-LACO-OFDM, RI-IDFTS and HTP-LACO-OFDM as a function of alphabet cardinality, M. The number of subcarrier used are $N = 2048$. Here, the PAPR results of RI-IDFTS are presented to demonstrate the improvement over the counterpart which includes HS. It can be observed that RI-IDFTS manifests considerably lower PAPR compared to LACO-OFDM and FTP-LACO-OFDM, however, only a marginal improvement is observed over HTP-LACO-OFDM. As shall become apparent in the subsequent sections, the augmentation in complexity of FTP-LACO-OFDM and RI-IDFTS would significantly overshadow the usefulness. Additionally, the real-imaginary component interference and synchronization issue would further impede the performance of RI-IDFTS. Another important observation that can be drawn from Fig. 16 is that the PAPR of both FTP-LACO-OFDM and HTP-LACO-OFDM reaches a constant value for $M \geq 64$.

4.7. Optical Power Penalty

For a given BER, P_{b}, optical power penalty can be obtained by normalizing the expected optical power by the average optical power required for OOK in an AWGN channel without bandwidth limitation, i.e., $E^{\text{OOK}}_{\text{b(opt)}}/N_0$. $E^{\text{OOK}}_{\text{b(opt)}}/N_0$ to reach P_{b} is obtained as $\text{erfc}^{-2}(2P_{\text{b}})$, where $\text{erfc}(\cdot)$ is the complementary error function. Considering a time dispersive channel, $P_{\text{b}} = 10^{-3}$, and $\eta_{(\cdot)} \approx \{1, 2\}$ bits/s/Hz, the optical power penalty is evaluated by altering the ratio of data-rate to the 3 dB LED cut-off frequency, i.e., $R_{\text{b}}/f_{\text{3dB}}$, as rendered in Fig. 17 and Fig. 18. The results reveal that LACO-OFDM incurs the most optical power penalty for high data-rates. On the other hand, FTP-LACO-OFDM experiences the lowest optical power penalty whilst, HTP-LACO-OFDM incurs a marginal increase in penalty over FTP-LACO-OFDM for high data-rates. Lower penalty for the

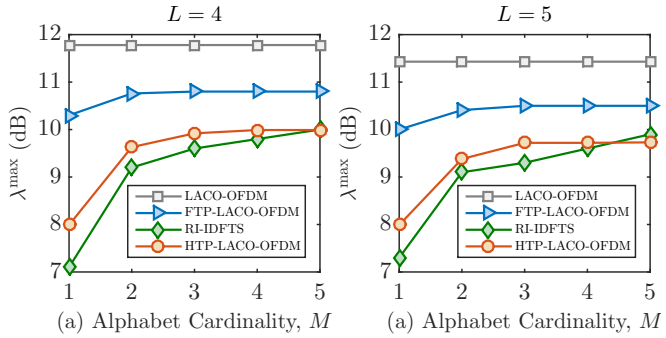

Figure 16: PAPR at CCDF = 0.1 as a function of M for LACO-OFDM, FTP-LACO-OFDM, RI-IDFTS and HTP-LACO-OFDM: (a) $L = 4$; (b) $L = 5$.

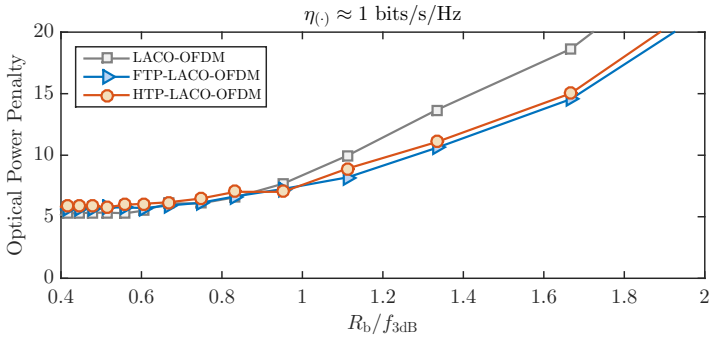

Figure 17: Optical power penalties of LACO-OFDM, FTP-LACO-OFDM and HTP-LACO-OFDM for $\eta_{(\cdot)} \approx 1$ bits/s/Hz.

precoded methods for the high data-rates is because of precoding, while, for low data-rates, optical power penalties of all the layered approaches are virtually the same.

4.8. Complexity Analysis

The complexities of LACO-OFDM, FTP-LACO-OFDM and HTP-LACO-OFDM are assessed by computing the number of prescribed arithmetic operations at the transceiver. For these approaches, the complexity is due to the equalization and due to the DFT/IDFT, DHT/IDHT needed. As aforementioned, the equalization complexity for both these approaches is the same, henceforth, in the sequel, only the complexities incurred due to the DFT/IDFT and DHT/IDHT would be considered. DFT and IDFT are executed using fast Fourier transform (FFT) and inverse FFT (IFFT) algorithms, respectively. An N-order FFT/IFFT approximately requires $4N\log_2(N)$ arithmetic operations [31], while N-order DHT/IDHT nearly requires $2N\log_2(N)$ arithmetic operations [32]. So, LACO-OFDM, and FTP-LACO-OFDM (same complexity as RI-IDFTS) would require

$$\mathcal{C}_{\text{LACO}} = 4N\log_2(N)[3L-1], \tag{56}$$

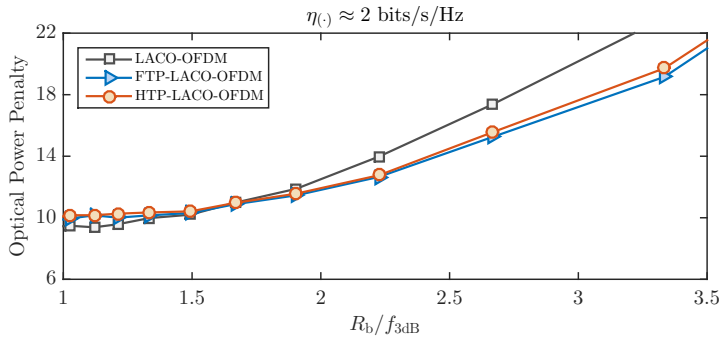

Figure 18: Optical power penalties of LACO-OFDM, FTP-LACO-OFDM and HTP-LACO-OFDM for $\eta_{(\cdot)} \approx 2$ bits/s/Hz

and

$$\begin{aligned}\mathcal{C}_{\text{FTP}} = 4N\log_2(N)[3L-1] + \left(\frac{N}{2^{L-2}}\right)[\log_2(N) - L - 1] \\ + 12\sum_{l=1}^{L-1}\left(\frac{N}{2^{l+1}}\right)\log_2\left(\frac{N}{2^{l+1}}\right),\end{aligned} \tag{57}$$

arithmetic operations, respectively. By taking into account the complexity imposed by DHT/IDHT, HTP-LACO-OFDM requires

$$\begin{aligned}\mathcal{C}_{\text{LDHTS}} = 2N\log_2(N)[3L-1] + \left(\frac{N}{2^{L-2}}\right)[\log_2(N) - L] \\ + 6\sum_{l=1}^{L-1}\left(\frac{N}{2^{l}}\right)\log_2\left(\frac{N}{2^{l}}\right),\end{aligned} \tag{58}$$

operations. From (56) and (57), it is evident that the complexity of LACO-OFDM is less than FTP-LACO-OFDM (or RI-IDFTS) because additional operations are required owing to the precoding and decoding required at the transmitter and the receiver, respectively. While, contrasting (58) with (57) and (56), it can be realized that HTP-LACO-OFDM features the least complexity. To emphasize the reduction in complexity for HTP-LACO-OFDM, we introduce relative gain parameters as:

$$\hat{\mathcal{G}}(N,L) = \left[1 - \frac{\mathcal{C}_{\text{HTP}}}{\mathcal{C}_{\text{LACO}}}\right] \times 100\%, \tag{59}$$

and

$$\tilde{\mathcal{G}}(N,L) = \left[1 - \frac{\mathcal{C}_{\text{HTP}}}{\mathcal{C}_{\text{FTP}}}\right] \times 100\%. \tag{60}$$

$\hat{\mathcal{G}}(N,L)$ measures the relative complexity reduction of HTP-LACO-OFDM over LACO-OFDM, while $\tilde{\mathcal{G}}(N,L)$ classifies the reduction in complexity for HTP-LACO-OFDM over FTP-LACO-

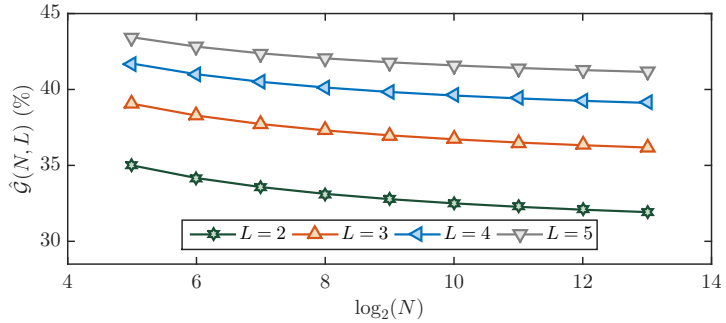

Figure 19: Relative complexity gain of HTP-LACO-OFDM over LACO-OFDM.

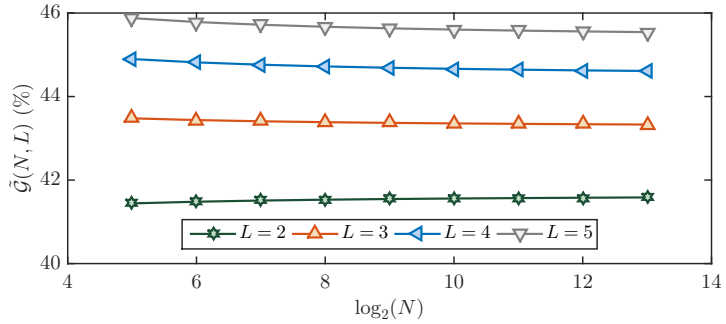

Figure 20: Relative complexity gain of HTP-LACO-OFDM over FTP-LACO-OFDM.

OFDM (or RI-IDFTS).

$\hat{\mathcal{G}}(N,L)$ as a function of layers, L is illustrated in Fig. 19 which proves that HTP-LACO-OFDM is appreciably less complex than LACO-OFDM. Besides, the gain increases with an increase in the number of superimposed layers, reaching $\approx 43\%$ for $\{L, \log_2(N)\} = 5$. Furthermore, $\tilde{\mathcal{G}}(L,N)$ considering different number of layers, L is graphically displayed in Fig. 20. It can be recognized that $\hat{\mathcal{G}}(N,L) < \tilde{\mathcal{G}}(N,L)$, e.g., in contrast to $\hat{\mathcal{G}}(32,5) \approx 43\%$, we have $\tilde{\mathcal{G}}(32,5) \approx 46\%$. It is again asserted that the two FT precoding variants of LACO-OFDM have been suggested in [21] involve the same amount of arithmetic operations; which are indeed higher than conventional LACO-OFDM and HTP-LACO-OFDM. This increment in complexity may outweigh the practicality because complexity is one of the primary limiting factors even for LACO-OFDM [14].

The complexities of all the approaches are assessed contemplating the implementation procedure adopted in the most recent article [9]. However, an implementation of LACO-OFDM and FTP-LACO-OFDM with lower order IDFT/DFT is presented in [8] and [21], respectively. While, the implementation of HTP-LACO-OFDM with lower order DHT is presented in [22].

5. Comparisons

Based on the performance of the studied approaches, following comparisons can be rendered:

1. For a given layer, the layering attenuation is less for LACO-OFDM compared to FTP-LACO-OFDM and HTP-LACO-OFDM. This entails that the BER degradation for LACO-OFDM is lesser than FTP-LACO-OFDM and HTP-LACO-OFDM in an AWGN channel (if no supplementary clipping from the LED is considered).
2. The electrical-to-optical power conversion efficiency for LACO-OFDM is better than FTP-LACO-OFDM and HTP-LACO-OFDM. Accordingly, the optical power consumption for LACO-OFDM is less compared to precoded variants in an AWGN channel.
3. In a time dispersive channel which mimics practical scenarios, the BER performances of precoded layered approaches are noticeably better than LACO-OFDM because of averaging effect of the decoder on the SNR. Among these approaches, FTP-LACO-OFDM marginally outperforms HTP-LACO-OFDM. Unfortunately, this averaging operation limits the use of bit loading for the precoded variants because all the subcarriers have the same SNR.
4. It has been identified that HS proceeds in an ineffective bandwidth usage for DCO-OFDM and ACO-OFDM compared to the unipolar base-band approaches, e.g. PAM [14]. LACO-OFDM and FTP-LACO-OFDM are also bandwidth inefficient because of HS is needed. However, for HTP-ACO-OFDM, as HS is no longer obliged, all the subcarriers can transmit data if sufficient layers are superimposed (theoretically $L = \infty$), thus alleviating the inefficient bandwidth efficiency problem. However, even then, the SE for HTP-LACO-OFDM cannot be increased due to the use of $\sqrt{M}$-ary PAM alphabets. On the other hand, RI-IDFTS also modulates the same number of subcarriers as that of counterpart with HS, hence, the SE is also the same as that of other approaches discussed.
5. Both precoded approaches manifest lower PAPR compared to LACO-OFDM, with RI-IDFTS featuring the least. However, the practicality of RI-IDFTS is questionable. The second best approach is HTP-LACO-OFDM. The lower PAPR of FTP-LACO-OFDM without HS and HTP-LACO-OFDM is foreseen because HS is no longer required. Several studies, e.g., [33] have indicated that HS leads toward an increase of PAPR because only half of the TD samples manifests single-carrier like properties. Hence, by excluding HS, PAPR is lowered as can be seen for RI-IDFTS and HTP-LACO-OFDM.
6. The system complexity of HTP-LACO-OFDM is less than both LACO-OFDM and FTP-LACO-OFDM. FTP-LACO-OFDM (or RI-IDFTS) demonstrate the highest complexity. It is necessary to highlight here that even though RI-IDFTS permits a lower PAPR; the complexity is overwhelmingly significant compared to both LACO-OFDM and HTP-LACO-OFDM because of complex equalization process and synchronization issues.

6. Conclusion

In this work, the performance of precoded and non-precoded LACO-OFDM approaches is appraised. The BER performance of LACO-OFDM is better than that of precoded approaches in an AWGN channel because of lesser layereing attenuation compared to other alternatives. Moreover, the BER performance of FTP-LACO-OFDM is somewhat better than HTP-LACO-OFDM because

the latter approach culminates the highest increase in SNR because of superimposed structure. However, in a time dispersive channel, the precoded approaches, that are, FTP-LACO-OFDM and HTP-LACO-OFDM, result in a superior BER performance because of averaging impact of decoder on the SNR. Furthermore, precoded LACO-OFDM approaches exhibit lower PAPR compared to LACO-OFDM. Among the precoded approaches, HTP-LACO-OFDM demonstrates the lowest PAPR because of precoding and by averting the HS. Besides, the complexity of FTP-LACO-OFDM (or RI-IDFTS) is higher than LACO-OFDM, the ramifications of which dominate other enhancements. Howbeit, the complexity of HTP-LACO-OFDM is lesser compared to LACO-OFDM. Unlike LACO-OFDM and FTP-LACO-OFDM, HTP-LACO-OFDM offers efficient bandwidth utilization. Hence, it can be concluded that HTP-LACO-OFDM can be a formidable substitute to LACO-OFDM for VLC systems because of enhanced BER, lower PAPR, lesser sensitivity to non-linear distortions, lower computational complexity and efficient bandwidth usage.

References

[1] D. Karunatilaka, F. Zafar, V. Kalavally, and R. Parthiban. LED based indoor visible light communications: State of the art. *IEEE Commun. Surv. Tut.*, 17(3):1649–1678, 2015.

[2] Carruthers J. B. and J. M. Kahn. Multiple-subcarrier modulation for nondirected wireless infrared communication. *IEEE J. Sel. Areas Commun.*, 14(3):538–546, 1996.

[3] J. Armstrong and A. J. Lower. Power efficient optical OFDM. *Electron. Lett*, 42(6):370–372, 2006.

[4] J. Armstrong. OFDM for optical communications. *J. Lightw. Tech.*, 27(3):189–204, 2009.

[5] H. Elgala, R. Mesleh, and H. Haas. Indoor optical wireless communication: potential and state-of-the-art. *IEEE Commun. Mag.*, 49(9), 2011.

[6] N. Fernando, Y. Hong, and E. Viterbo. Flip-OFDM for unipolar communication systems. *IEEE Trans. Commun.*, 60(12):3726–3733, 2012.

[7] D. Tsonev, S. Sinanovic, and H. Haas. Novel unipolar orthogonal frequency division multiplexing (U-OFDM) for optical wireless. *IEEE Veh. Tech. Conf.*, pages 1–5, 2012.

[8] Q. Wang, C. Qian, X. Guo, Z. Wang, D. G. Cunningham, and I. H. White. Layered ACO-OFDM for intensity-modulated direct-detection optical wireless transmission. *Opt. Express*, 23(9):12382–12393, 2015.

[9] X. Zhang, R. Wang, Q.and Zhang, S. Chen, and L. Hanzo. Performance analysis of layered ACO-OFDM. *IEEE Access*, 5:18366–18381, 2017.

[10] M. S. Islim and H. Haas. Augmenting the spectral efficiency of enhanced PAM-DMT-based optical wireless communications. *Opt. Express*, 24(11):11932–11949, 2016.

[11] D. Tsonev, S. Videv, and H. Haas. Unlocking spectral efficiency in intensity modulation and direct detection systems. *IEEE J. Selec. Areas Commun.*, 33(9):1758–1770, 2015.

[12] A. J. Lowery. Comparisons of spectrally-enhanced asymmetrically-clipped optical OFDM systems. *Opt. Express*, 24(4):3950–3966, 2016.

[13] A. W. Azim, Y. Le Guennec, and G. Maury. Decision-directed iterative methods for PAPR reduction in optical wireless OFDM systems. *Opt. Commun.*, 389:318–330, 2017.

[14] M. A. Khalighi, S. Long, S. Bourennane, and Z. Ghassemlooy. PAM and CAP-based transmission schemes for visible-light communications. *IEEE Access*, 2017.

[15] W. O. Popoola, Z. Ghassemlooy, and B. G. Stewart. Pilot-assisted PAPR reduction technique for optical OFDM communication systems. *J. Lightw. Tech.*, 32(7):1374–1382, 2014.

[16] L. Nadal, M. S. Moreolo, J. M. Fabrega, and G. Junyent. Comparison of peak power reduction techniques in optical OFDM systems based on FFT and FHT. *Intl. Conf. on Transparent Opt. Networks*, pages 1–4, 2011.

[17] K. Acolatse, Y. Bar-Ness, and S. K. Wilson. Novel techniques of single-carrier frequency-domain equalization for optical wireless communications. *EURASIP J. Adv. Sig. Process.*, 2011:1–13, 2011.

[18] R. Mesleh, H. Elgala, and H. Haas. LED nonlinearity mitigation techniques in optical wireless OFDM communication systems. *J. Opt. Commun. and Netw.*, 4(11):865–875, 2012.

[19] B. Ranjha, Z. Zhou, and M. Kavehrad. Performance analysis of precoding-based asymmetrically clipped optical orthogonal frequency division multiplexing wireless system in additive white Gaussian noise and indoor multipath channel. *Opt. Eng.*, 53(8):086102–086102, 2014.

[20] J. Zhou and Y. Qiao. Low-PAPR asymmetrically clipped optical OFDM for intensity-modulation/direct-detection systems. *IEEE Photon. J.*, 7(3):1–8, 2015.

[21] R. Bai, Z. Wang, R. Jiang, and J. Cheng. Interleaved DFT-spread layered/enhanced ACO-OFDM for Intensity-Modulated Direct-Detection systems. *J. Lightw. Tech.*, 36(20):4713–4722, 2018.

[22] J. Zhou, Q. Wang, Q. Cheng, M. Guo, Y. Lu, A. Yang, and Y. Qiao. Low-PAPR layered/enhanced ACO-SCFDM for optical-wireless communications. *IEEE Photon. Techn. Lett.,*, 30(2):165–168, 2018.

[23] A. W. Azim, Y. Le Guennec, and G. Maury. Spectrally augmented Hartley transform precoded asymmetrically clipped optical OFDM for VLC. *IEEE Photon. Techn. Lett.,*, 30(23):2029–2032, 2018.

[24] F. Barrami, Y. Le Guennec, E. Novakov, J.-M. Duchamp, and P. Busson. A novel FFT/IFFT size efficient technique to generate real time optical OFDM signals compatible with IM/DD systems. *Euro. Microw. Conf.*, pages 1247–1250, 2013.

[25] A. Weiss, A. Yeredor, and M. Shtaif. Iterative symbol recovery for power-efficient DC-biased optical OFDM systems. *J. Lightw. Tech.*, 34(9):2331–2338, 2016.

[26] H. Elgala, R. Mesleh, and H. Haas. Non-linearity effects and predistortion in optical OFDM wireless transmission using LEDs. *Intl. J. Ultra Wideband Commun. Syst.*, 1(2):143–150, 2009.

[27] R. N. Bracewell. Discrete Hartley transform. *JOSA*, 73(12):1832–1835, 1983.

[28] J. Armstrong and B. J. C. Schmidt. Comparison of asymmetrically clipped optical OFDM and DC-biased optical OFDM in AWGN. *IEEE Commun. Lett.*, 12(5):343–345, 2008.

[29] M. Wolf, S. A. Cheema, M. A. Khalighi, and S. Long. Transmission schemes for visible light communications in multipath environments. *Intl. Conf. on Transparent Opt. Networks*, pages 1–7, 2015.

[30] K. Lee, H. Park, and J. R. Barry. Indoor channel characteristics for visible light communications. *IEEE Commun. Lett.*, 15(2):217–219, 2011.

[31] S. G. Johnson and M. Frigo. A modified split-radix FFT with fewer arithmetic operations. *IEEE Trans. Sig. Process.*, 55(1):111–119, 2007.

[32] J. Zhou, Y. Qiao, Z. Cai, and Y. Ji. An improved scheme for flip-OFDM based on Hartley transform in short-range IM/DD systems. *Opt. Express*, 22(17):20748–20756, 2014.

[33] C. Wu, H. Zhang, and W. Xu. On visible light communication using LED array with DFT-spread OFDM. *IEEE ICC*, pages 3325–3330, 2014.